Polyhedron 151 (2018) 100–111

Contents lists available at ScienceDirect

Polyhedron

journal homepage: www.elsevier.com/locate/poly

# Nitric oxide photo-release from a ruthenium nitrosyl complex with a 4,4′-bisfluorenyl-2,2′-bipyridine ligand

Max Roose [a], Isabelle Sasaki [a], Valerii Bukhanko [a], Sonia Mallet-Ladeira [a], Rodrigo M. Barba-Barba [b], Gabriel Ramos-Ortiz [b], Alejandro Enriquez-Cabrera [c], Norberto Farfán [c], Pascal G. Lacroix [a,*], Isabelle Malfant [a,*]

[a] CNRS, Laboratoire de Chimie de Coordination (LCC) du CNRS, 205 route de Narbonne, BP44099, Toulouse Cedex 4 31077, France
[b] Centro de Investigaciones en Óptica (CIO), A.P. 1-948, 37000 León, Gto, Mexico
[c] Facultad de Quimica, Departamento de Quimica Orgánica, Universidad Nacional Autónoma de México, 04510 México D.F., Mexico

ARTICLE INFO

*Article history:*
Received 3 April 2018
Accepted 12 May 2018
Available online 22 May 2018

*Keywords:*
Nitric oxide
Ruthenium complexes
Two-photon absorption
Photochemistry
DFT computations

ABSTRACT

A ruthenium nitrosyl complex of formula $[Ru^{II}(terpy)(F2B)(NO)](PF_6)_3$, where terpy stands for 2,2′:6′,2″-terpyridine and F2B for 4,4′-bis(9,9′-dibutyl-9H-fluoren-2-yl)-2,2′-bipyridine, is presented and fully characterized. The X-ray crystal structure of F2B is reported. The electronic properties of the complex are compared to those of related $[Ru^{II}(terpy)(bpy)(NO)]^{3+}$ complexes having a bipyridine (bpy) free of fluorene or bearing a fluorene on the terpyridine ligand. DFT computations are provided to support the experimental data. $[Ru^{II}(terpy)(F2B)(NO)](PF_6)_3$ releases NO under irradiation at 405 nm with a quantum yield ($\phi_{NO}$) equal to 0.033. Additionally, the two-photon absorption cross-section investigated at 800 nm by the Z-scan technics is equal to 156 ± 23 GM, which indicates that the complex can release NO under irradiation in the therapeutic window.



## 1. Introduction

Nitric oxide (NO) has been attracting a growing interest in relation to its biological functions and possible therapeutic applications [1,2]. NO is classified as a messenger molecule involved in various biochemical and physiological processes, such as stimulation of the immune and endocrine response, blood pressure regulation, neurotransmission, and action in the cells developments [3,4].

However, its concentration in the cellular environment is considered an important factor for its biological action. For instance nanomolar concentrations can promote cells growth with applications in tissues healing, and micromolar concentrations induce cells death by apoptosis with applications in anti-cancer therapies [5–7]. In this context, exogenous NO donors have become widely investigated, but their relevance has to be evaluated on the basis of their ability to deliver NO locally and quantitatively, in order to avoid undesirable effects on untargeted cells. Among potential candidates, various metal-nitrosyl complexes have been envisioned [8], such as iron [9], and manganese [10] based materials. Nevertheless, ruthenium-nitrosyl complexes have gradually been recognized as the most promising NO donors in relation to their low cytotoxicity towards host cells, good stability in water when compared to iron and manganese complexes, and moreover their capability of releasing NO under light irradiation in the $\lambda$ = 300–600 nm domain, exclusively, taking advantage of the noninvasive and highly controllable characteristics of light [11–13]. However, to be fully applicable, the photochemically induced NO release should be achieved in the 600–1300 nm therapeutic window, of relative transparency of the biological media [14].

To overpass this difficulty and to design alternative NO donors compatible with the therapeutic window, we have recently reported on $[Ru^{II}(FT)(bpy)(NO)](PF_6)_3$ ($[\mathbf{1}](PF_6)_3$) in which the ruthenium nitrosyl complex ($[\mathbf{1}]^{3+}$ in Scheme 1), is built up from the 4′-(2-fluorenyl)-2,2′:6′,2″-terpyridine (FT) ligand [15]. The introduction of a fluorene unit on the $[Ru^{II}$(terpyridine(bipyridine)(NO)] core is motivated by the widely reported capabilities of fluorene to enhance the two-photon absorption (TPA) properties of molecules [16]. Indeed, the TPA approach offers the most appealing perspectives in photodynamic therapy [17,18]: (*i*) high level of spatial resolution arising from its quadratic dependence on the pulsed light intensity; (*ii*) possibility to replace one photon in the visible domain by two photons in the near-infrared therapeutic window allowing more penetration depth in tissue; (*iii*)

* Corresponding authors.
*E-mail addresses:* pascal.lacroix@lcc-toulouse.fr (P.G. Lacroix), isabelle.malfant@lcc-toulouse.fr (I. Malfant).

https://doi.org/10.1016/j.poly.2018.05.028
0277-5387/

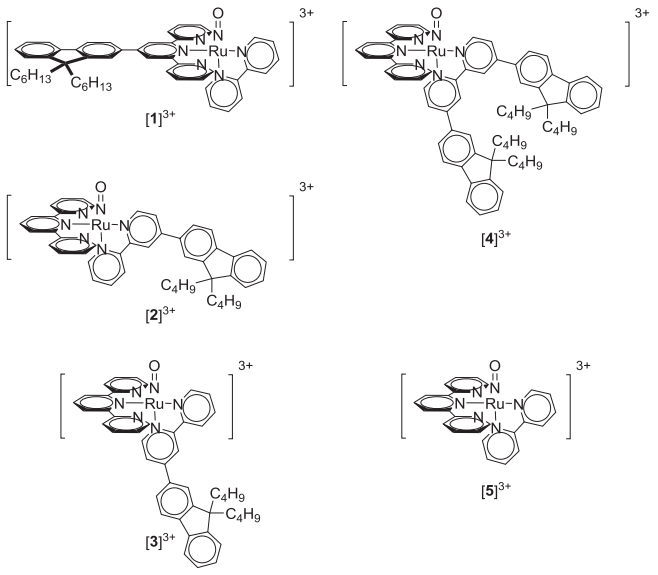


**Scheme 1.** Molecular formula for the ruthenium nitrosyl complexes under investigation.

reduced side effects due to the absence of UV radiation and to the use of ultra-short laser pulses. In a continuous effort aimed at investigating ruthenium nitrosyl complexes with enhanced capabilities, we wish now to report on related species containing the fluorene unit on the bipyridine instead of the terpyridine ligand. The anticipated candidates are the complex isomers $[\mathbf{2}]^{3+}$ and $[\mathbf{3}]^{3+}$ (Scheme 1), which differ by the position of the fluorene substituent either in *cis*- ($[\mathbf{2}]^{3+}$) or *trans*- ($[\mathbf{3}]^{3+}$) position, with respect to the Ru(NO) group.

The organization of the present manuscript will be the following: (*i*) a computational investigation carried out by the Density Functional Theory (DFT) method will be presented first for the three complexes $[\mathbf{1}]^{3+}$, $[\mathbf{2}]^{3+}$, and $[\mathbf{3}]^{3+}$, and extended to complex $[\mathbf{4}]^{3+}$ (Scheme 1) in which two fluorenes are present on the bipyridine ligand, and to complex $[\mathbf{5}]^{3+}$, free of fluorene, in order to fully understand the scope and limitation of the fluorene-based methodology, and to identify the most promising synthetic target; (*ii*) the synthesis and full characterization of the selected $[\mathbf{4}](PF_6)_3$ compound will be reported with the X-ray crystal structure of the bipyridine ligand substituted by two fluorene units (F2B); (*iii*) the following sections will be devoted to a comparison of the optical properties of $[\mathbf{4}](PF_6)_3$ with those of $[\mathbf{1}](PF_6)_3$ and $[\mathbf{5}](PF_6)_3$ at one (UV–Vis spectroscopy) and two-photon (TPA) in relation to the NO release capabilities, expressed as the quantum yield ($\phi_{NO}$) of photo release under irradiation.

## 2. Experimental

### 2.1. Starting materials and equipment

The F2B ligand was synthesized as previously described in the literature [19] $[Ru^{II}(terpy)(bpy)(NO)](PF_6)_3$ was synthesized as previously reported [20], as was $[Ru^{II}(terpy)Cl_3]$ [21]. Triethylamine (Sigma–Aldrich), LiCl (Alfa Aesar), Ethylene glycol (Fluka), $NH_4PF_6$ (Alfa Aesar), and $NaNO_2$ (Fluka) were the highest purity grade and were used as received. The UV–Vis spectra were obtained on a Hewlett Packard 8454A spectrometer. Electron paramagnetic resonance experiments (EPR) were performed on a Brucker ESP 500E spectrometer. The following setting was employed for the measurements: microwave power, 20 mW, field modulation amplitude, 0.1 mT; field modulation frequency, 100 kHz; microwave frequency, 9.497392 GHz. N-methyl-D-glucamine dithiocarbamate previously synthetized reacted with Mohr salts to get $[Fe(MGD)_2]$ [32]. 90 μL of 1 mM of $[\mathbf{4}](PF_6)_3$ in acetonitrile and 8 μL of $HPF_6$ were mixed with 10 μL of a 2 mM aqueous solution of $[Fe(MGD)_2]$ and injected into quartz capillaries. Samples were irradiated directly in the EPR cavity. The light source was a 250 W Oriel Hg lamp (Palaiseau, France). The light was passed through an Oriel WG 400 UV filter (Palaiseau, France, $\lambda > 400$ nm) and delivered *via* an optical fiber to the grid of the cavity.

### 2.2. Synthesis

*$[Ru^{II}(terpy)(F2B)(Cl)](Cl)$.* F2B (142 mg, 0.2 mmol), $[Ru^{III}(terpy)Cl_3]$ (88 mg, 0.2 mmol), LiCl (64 mg, 1.5 mmol), ethylene glycol (27 mL), and triethylamine (0.24 mL, 1.7 mmol) were successively added in a 100 mL flask and heated under reflux for two days. The reaction mixture was cooled down to room temperature, filtered, and evaporated to dryness under reduced pressure. The residue was dispersed in 100 mL of water, stirred and finally filtered and dried under vacuum affording 144 mg (64% yield) of a black purple solid. $^1$H NMR (MeOD, 400 MHz): $\delta$ 10.24 ppm (1H, d, $H_{6bpy}$, $^3J_{6/5}$ = 6.0 Hz), 9.28 (1H, s, $H_{3bpy}$), 8.98 (1H, s, $H_{3'bpy}$), 8.68 (2H, d, $H_{3'tpy}$ + $H_{5'tpy}$, $^3J_{3'/4'} = {}^3J_{5'/4'}$ = 8.1 Hz), 8.56 (2H, d, $H_3$ + $H_{3''tpy}$, $^3J_{3/4} = {}^3J_{3''/4''}$ = 8.1 Hz), 8.40 (1H, m, $H_{5bpy}$), 8.24–8.17 (3H, m, $H_{1Fl}$ + $H_{3Fl}$ + $H_{4'tpy}$), 8.06 (1H, d, $H_{4Fl}$, $^3J_{4/3}$ = 8.1 Hz), 7.97–7.77 (9H, m, $H_{4tpy}$ + $H_{4''tpy}$ + $H_{6tpy}$ + $H_{6''tpy}$ + $H_{5Fl}$ + $H_{6Fl}$ + $H_{7Fl}$ + $H_{8Fl}$ + $H_{6'bpy}$), 7.49–7.34 (10H, m, $H_{5'Fl}$ + $H_{6'Fl}$ + $H_{7'Fl}$ + $H_{8'Fl}$ + $H_{5/5''tpy}$ + $H_{5'bpy}$ + $H_{1'Fl}$ + $H_{3'Fl}$ + $H_{4'Fl}$), 2.20–2.03 (8H, m, 4 $CH_{2\alpha}$), 1.18–0.99 (8H, m, 4 $CH_{2\gamma}$), 0.73–0.46 (16H, m, 4 CH3δ+4 $CH_{2\beta}$). IR: $\nu$: 3063 cm$^{-1}$ ($\nu_{arom}$), 2953 ($\nu_{alkyle}$), 2926 ($\nu_{alkyle}$), 2858 ($\nu_{alkyle}$), 1714, 1604, 1447 ($\nu_{arom}$), 1386, 1281, 1246, 1079, 1049, 1022, 885, 828, 769 ($\nu_{arom}$), 739 ($\nu_{arom}$), 424. ESI-MS: m/z: 1078.8 [$(M-Cl)^+$]. UV–Vis ($CH_3CN$): $\lambda_{max}$: 235 nm (sh), 280, 307, 318, 350 (sh), 516.

*$[Ru^{II}(terpy)(F2B)(NO_2)](PF_6)$.* $[Ru^{II}(terpy)(F2B)(Cl)](Cl)$ (127 mg, 0.11 mmol) was dissolved in a mixture of ethanol (7.5 mL) and water (2.5 mL). After complete dissolution, $NaNO_2$ (75 mg, 1.05 mmol) was added, then the reaction mixture was heated to reflux, for 3.5 h. After cooling down to room temperature, an excess of $NH_4PF_6$ (240 mg, 1.47 mmol) dissolved in 1 mL of water was added. After concentration of the reaction mixture to 75% of its initial volume, the resulting solution was placed in a fridge overnight, which led to the appearance of a dark brown solid. Filtration and drying under vacuum provided 102 mg (75% yield) of the desired compound. $^1$H NMR ($CD_3CN$, 400 MHz): $\delta$ 9.92 (1H, d, $H_{6bpy}$, $^3J_{6/5}$ = 6.0 Hz), 9.13 (1H, d, $H_{3bpy}$, $^4J_{3/5}$ = 2.0 Hz), 8.89 (1H, d, $H_{3'bpy}$, $^4J_{3'/5'}$ = 1.8 Hz), 8.52 (2H, d, $H_{3'tpy}$ + $H_{5'tpy}$, $^3J_{3'/4'} = {}^3J_{5'/4'}$ = 8.1 Hz), 8.40 (2H, d, $H_{3tpy}$ + $H_{3''tpy}$, $^3J_{3/4} = {}^3J_{3''/4''}$ = 8.1 Hz), 8.37 (1H, dd, $H_{5bpy}$, $^3J_{5/6}$ = 6.0 Hz, $^4J_{5/3}$ = 2.0 Hz), 8.25–8.16 (3H, m, $H_{4'tpy}$ + $H_{1Fl}$ + $H_{3Fl}$), 8.06 (1H, d, $H_{4Fl}$, $^3J_{4/3}$ = 8.0 Hz), 7.97 (2H, m, $H_{4tpy}$ + $H_{4''tpy}$), 7.93–7.77 (9H, m, $H_{6tpy}$ + $H_{6''tpy}$ + $H_{6'bpy}$ + $H_{5Fl}$ + $H_{6Fl}$ + $H_{7Fl}$ + $H_{8Fl}$), 7.54–7.32 (10H, m, $H_{5'bpy}$ + $H_{5tpy}$ + $H_{5''tpy}$ + $H_{1'Fl}$ + $H_{3'Fl}$ + $H_{4'Fl}$ + $H_{5'Fl}$ + $H_{6'Fl}$ + $H_{7'Fl}$ + $H_{8'Fl}$), 1.17–1.01 (8H, m, 4 $CH_{2\gamma)}$, 0.70(6H, t, 2 CH3δ, $^3J\delta/_\gamma$ = 7.3 Hz), 0.69–0.58 (10H, m, 2 $CH_{3\delta+2}$ $CH_{2\beta}$), 0.47 (4H, m, 2 $CH_{2\beta)}$. The protons in alpha position of the butyl chains are hidden under the peak of water at around 2.1 ppm. IR: $\nu$(cm$^{-1}$): 2955 ($\nu_{alkyle}$), 2928 ($\nu_{alkyle}$), 2858 ($\nu_{alkyle}$), 1606, 1466 ($\nu_{arom}$), 1450 ($\nu_{arom}$), 1388, 1342 ($\nu_{NO2}$), 1299, 1283, 839 ($\nu_{PF6}$), 772 ($\nu_{arom}$), 742 ($\nu_{arom}$), 556 ($\nu_{PF6}$). ESI-MS: m/z: 1089.7 [$(M-NO_2)^+$]. UV–Vis ($CH_3CN$): $\lambda_{max}$ (ε): 272 nm (sh), 281 (39 000 mol$^{-1}$ L cm$^{-1}$), 306 (49 000), 328, 354 (sh), 487 (16 000).

*$[Ru^{II}(terpy)(F2B)(NO)](PF_6)_3$* ($[\mathbf{4}](PF_6)_3$). $[Ru^{II}(terpy)(F2B)(NO_2)](PF_6)$ (66 mg, 0.054 mmol) was dissolved in a mixture of ethanol (30 mL) and hydrochloric acid 37% (4.9 mL). The resulting solution was heated at 60 °C for one hour. The mixture was let to reach room temperature, then $NH_4PF_6$ (300 mg 1.84 mmol) dissolved in 3 mL of water were added. The resulting solution was concentrated

under vacuum, at a temperature maintained below 30 °C, until a beginning of precipitation occurred. The flask when then left in a fridge for one day. After filtration, the resulting light brown solid was washed with cold water, and dried under vacuum (69 mg, 85%). $^1$H NMR ($CD_3CN$, 400 MHz): $\delta$ 9.29 ppm (1H, d, $H_{3bpy}$, $^4J_{3/5}$ = 2.1 Hz), 9.28 (1H, d, $H_{6bpy}$, $^3J_{6/5}$ = 6.2 Hz), 9.08 (1H, d, $H_{3'bpy}$, $^4J_{3'/5'}$ = 2.1 Hz), 9.00 (1H, m), 8.91 (1H, s), 8.89 (1H, d, J = 1.11 Hz), 8.74 (2H, dd, $H_{3tpy}$ + $H_{3''tpy}$, $^3J_{3/4}$ = $^3J_{3''/4''}$ = 8.2 Hz, $^4J_{3/5}$ = $^4J_{3''/5''}$ = 1.3 Hz), 8.60 (1H, dd, $H_{5bpy}$, $^3J_{5/6}$ = 6.2 Hz, $^4J_{5/3}$ = 2.0 Hz), 8.48 (2H, td, $H_{4tpy}$ + $H_{4''tpy}$, $^3J$ = 8.0 Hz, $^4J$ = 1.4 Hz), 8.29 (1H, d, J = 1.8 Hz), 8.25 (1H, dd, $^3J$ = 8.0 Hz, $^4J$ = 1.8 Hz), 8.20 (2H, dd, $H_{6tpy}$ + $H_{6''tpy}$, $^3J_{6/5}$ = $^3J_{6''/5''}$ = 5.7 Hz, $^4J_{6/4}$ = $^4J_{6''/4''}$ = 1.4 Hz), 8.12 (1H, d, $^3J$ = 8.0 Hz), 7.97–7.83 (6H, m), 7.79–7.73 (3H, m), 7.56–7.52 (1H, m), 7.48–7.35 (7H, m), 7.16 (1H, d, $H_{5'bpy}$, $^3J$ = 6.4 Hz), 2.32–2.04 (8H, m, 4 $CH_{2\alpha}$), 1.18–0.99 (8H, m, 4 $CH_{2\gamma}$), 0.71–0.55 (16H, m, 4 CH3$\delta$+2 $CH_{2\beta}$), 0.46 (4H, m, 2 $CH_{2\beta}$). $^{13}$C NMR ($CDCl_3$, 100 MHz): $\delta$ 156.7; 155.6; 155.0; 154.7; 154.6; 154.2; 153.6; 152.8; 152.5; 152.3; 151.6; 151.3; 147.5; 147.0; 145.5; 145.3; 144.4; 139.8; 139.6; 132.8; 132.4; 130.3; 128.8; 128.7; 128.3; 127.7; 127.5; 127.4; 127.4; 127.4; 127.0; 126.2; 124.0; 123.4; 123.3; 122.6; 121.9; 120.9; 120.8; 120.7; 120.6; 120.4; 55.6; 55.5; 39.6; 39.4; 31.6; 29.3; 29.1; 26.1; 25.9; 22.7; 22.6; 22.4; 13.4; 13.4; 13.2; 13.2; 13.1. IR: $\nu$(cm$^{-1}$): 2955 ($\nu_{alkyle}$), 2928 ($\nu_{alkyle}$), 2858 ($\nu_{alkyle}$), 1943 ($\nu_{NO}$), 1604, 1480 ($\nu_{arom}$), 1453 ($\nu_{arom}$), 1324, 1283, 1251, 1030, 836 ($\nu_{PF6}$), 772 ($\nu_{arom}$), 739 ($\nu_{arom}$), 556 ($\nu_{PF6}$), 422. ESI-MS: m/z: 537.4 [($Ru^{II}$-NO·)/2]; 710.0; 1089.6 [($Ru^{II}$-$NO_2$)$^+$]. UV–Vis ($CH_3CN$): $\lambda_{max}$ ($\varepsilon$): 306 nm (48 000 mol$^{-1}$ L cm$^{-1}$), 365 (39 000), 460 (sh). *Anal.* Calc. for $C_{67}H_{67}N_6ORuP_3F_{18}$: C, 53.35; H, 4.48; N, 5.57. Found: C, 54.92; H, 4.66; N, 5.18.

### 2.3. Crystallographic data for F2B

Single crystals suitable for X-ray diffraction studies were grown by slow diffusion of ether into a concentrated solution of F2B in acetonitrile. Data were collected at low temperature (100(2) K) on a Bruker Kappa Apex II diffractometer equipped with a 30 W air-cooled microfocus, using MoK$\alpha$ radiation ($\lambda$ = 0.71073 Å), and an Oxford Cryosystems Cryostream cooler device. Phi- and omega-scans were used for data collection. The structure was solved by intrinsic phasing method (SHELXT) [22]. All non-hydrogen atoms were refined anisotropically by means of least-squares procedures on $F^2$ with the aid of the program SHELXL [23]. All the hydrogen atoms were refined isotropically at calculated positions using a riding model. A maximum residual electron density is close to two carbon atoms and located at 1.076 Å from C16. Therefore such residual density is not an unaccounted atom and the thermal ellipsoids are not elongated to describe a disorder. The crystal structure of F2B has been deposited with the Cambridge Crystallographic Data Center.

$C_{52}H_{56}N_2$, $M$ = 708.99, monoclinic, $C$ 2/$c$, $a$ = 24.8759(8) Å, $b$ = 10.5669(3) Å, $c$ = 16.6085(6) Å, $\alpha$ = 90°, $\beta$ = 111.6820(10)°, $\gamma$ = 90°, $V$ = 4056.9(2) Å$^3$, $Z$ = 4, crystal size 0.20 × 0.18 × 0.12 mm$^3$, colourless block, 39 469 reflections collected (4478 independent, $R_{int}$ = 0.0412), 3812 reflections observed for $I > 2\sigma(I)$, Completeness to theta 25.242° = 99.9%, 246 parameters, $R1$ [$I > 2\sigma(I)$] = 0.0689, $wR2$ [all data] = 0.2013, largest difference peak and hole: 1.187 and −0.269 eÅ$^{-3}$. $R1 = \Sigma||F_o| - |F_c||/\Sigma|F_o|$, $wR2 = [\Sigma[w(F_o^2 - F_c^2)^2]/\Sigma[w(F_o^2)^2]]^{1/2}$.

### 2.4. Computational methods

The molecular geometries of the five [**1**]$^{3+}$–[**5**]$^{3+}$ complexes were fully optimized using the Gaussian-09 program package [24] within the framework of the DFT at the B3PW91/6-31G* level, the LANL2DZ pseudo-potential being used to account for relativistic effects on the ruthenium atom [25]. The butyl chains of each fluorene units were replaced by methyl groups in the computations to help reaching convergence. Vibrational analysis was performed at the same level to verify that the stationary points correspond to minima on the potential energy surfaces. The TD-DFT computations of the UV–Vis spectra were carried out on the optimized geometries at the CAM-B3LYP/6-31G* level. The DFT methods (B3PW91 and CAM-B3LYP) were selected to be consistent with our previous investigation of Ru(NO) complexes containing a fluorenylterpyridine ligand [26]. Molecular orbitals were plotted by using GABEDIT [27].

### 2.5. Electrochemistry

Electrochemical experiments were performed with a potentiostat Autolab PGSTAT100 (EcoChemie, The Netherlands) controlled by GPES 4.09 software. Experiments were carried out at room temperature in a homemade airtight three-electrode cell connected to a vacuum/argon line. The reference electrode was a saturated calomel electrode (SCE) separated from the solution by a bridge compartment. The counter electrode was a platinum wire of ca. 1 cm$^2$ apparent surface. The working electrode was a Pt microdisk (radius = 0.25 mm). The supporting electrolyte ($nBu_4N$)($PF_6$) (Fluka, 99% electrochemical grade) was used as received and simply degassed under argon. Acetonitrile was freshly purified prior to use. The solutions used during the electrochemical studies was $10^{-3}$ mol.L$^{-1}$ and $10^{-1}$ mol.L$^{-1}$ respectively for [**4**]($PF_6$)$_3$ and for the supporting electrolyte. Before each measurement, the solutions were degassed by bubbling argon through them, and the working electrode was polished with a polishing machine (Presi P230). Typical instrumental parameters for recorded square wave voltammograms were: SW frequency $f$ = 20 Hz, SW amplitude Esw = 20 mV, and scan increment dE = 5 mV.

### 2.6. NO photo release

*Photochemistry:* Kinetic studies on the photolysis reactions were carried out with a diode array Hewlett Packart 8454A spectrophotometer. Solutions of 2 mL of [**4**]($PF_6$)$_3$ ($2.85 \times 10^{-5}$ mol.L$^{-1}$) in non-deoxygenated acetonitrile were used. The optical fiber was fixed laterally from the cuvette. Absorption spectra were taken after each minute, in fast scan mode, during a period of 780 min for irradiation at 405 nm which allows reaching apparent stable absorption conditions. The UV–Vis spectra were recorded under irradiation realized with a Muller reactor device equipped with a cooling water filter and a mercury arc lamp equipped with appropriate interference filter to isolate the desired irradiation wavelength. The temperature was maintained at 25 °C during the whole experiment.

*Quantum yield measurements:* Light intensities were determined before each photolysis experiments by chemical actinometry procedure. The actinometer used was potassium ferrioxalate to $\lambda_{irr}$ = 405 nm ($I_0 = 1.52 \times 10^{-7}$ mol.L$^{-1}$.s$^{-1}$). The quantum yield ($\phi$A) for [**4**]($PF_6$)$_3$ was determined by the program Sa3.3 written by D. Lavabre and V. Pimienta [28]. It allows the resolution of the following differential equation:

$$\frac{d[A]}{dt} = -\Phi_A I_a^A = -\Phi_A Abs_A^{\lambda} I_0 F \quad (1)$$

where $I_a^A$ is the intensity of the light absorbed by the precursor; $Abs_A^{\lambda}$, the absorbance before irradiation; $Abs_{Tot}^{\lambda}$, the total absorbance; $I_0$, the incident intensity measured at 405 nm; and $F$, the photokinetic factor given by the following equation:

$$F = \frac{(1 - 10^{-Abs_{Tot}^{\lambda}})}{Abs_{Tot}^{\lambda}} \quad (2)$$

The equation was fitted with the experimental data $Abs^{\lambda}_{Tot} = f(t)$ and 2 parameters $\phi$A and $\varepsilon$B ($\varepsilon$B is the molar extinction coefficient measured at the end of the reaction) at two wavelengths ($\lambda_{irr}$=405 nm, $\lambda_{obs}$ = 470 nm). $\lambda_{obs}$ was chosen because it corresponds to a large difference between molar extinction coefficient at the initial and final time of the photochemical reaction. Simulation and optimization procedures were performed by using numerical integration and a non-linear minimization algorithm for the fitting of the model to the experimental data [28,29].

$$[A]_0 = 2.8510^{-5}\ \text{mol}\cdot\text{L}^{-1}, \quad \varepsilon_A^{405} = 23\,400\ \text{mol}^{-1}\cdot\text{L}\cdot\text{cm}^{-1},$$
$$\varepsilon_A^{470} = 9200\ \text{mol}^{-1}\cdot\text{L}\cdot\text{cm}^{-1}, \quad \varepsilon_B^{405} = 12\,400\ \text{mol}^{-1}\cdot\text{L}\cdot\text{cm}^{-1},$$
$$\varepsilon_B^{470} = 18\,400\ \text{mol}^{-1}\cdot\text{L}\cdot\text{cm}^{-1}$$

### 2.7. TPA experiments

The Z-scan technique was employed for the measurement of $\sigma_{TPA}$ [30]. The experimental apparatus was based on the same laser used in Ref. [30]. Briefly, the source of short optical pulses (100 fs) was a Ti:Sa regenerative amplifier (model Libra-HE-USP, Coherent) with emission at 800 nm and 1 kHz of repetition rate. The title compound [**4**](PF$_6$)$_3$ was tested at the concentration of $1 \times 10^{-2}$ mol.L$^{-1}$. Two energies were used in these experiments (73 and 100 nJ). The Z-scan apparatus was calibrated in close aperture measuring the nonlinear refractive index $n_2$ of the standard $CS_2$. Further, in open aperture condition, the apparatus was calibrated using rhodamine 6G (R6G) and rhodamine B (RB) as standards. Both, the close and open aperture conditions led values of nonlinearities for the standards in good agreement with literature [30,31]. The nonlinear absorption coefficient $\beta$ and TPA cross-section ($\sigma_{TPA}$) of the sample was obtained after fitting the normalized transmission $T(z)$ to Z-scan formalism [30].

## 3. Results and discussion

### 3.1. Selection of a synthetic target

The five [**1**]–[**5**] complexes under investigations have been optimized by DFT. The main geometrical data related to the coordination sphere of the ruthenium center are gathered in Table 1. The presence of fluorene does not affect significantly the coordination sphere around the ruthenium atom, except a tendency observed for a slight shortening of the Ru—N bond length, when the nitrogen atom belongs to a pyridine to which a fluorene is attached. Nevertheless, this shortening is limited to 0.5% in any case. More noticeable is the evolution of the torsion angle obtained between the averaged plane of the fluorene and that of the ligand (either terpyridine or bipyridine) from 29.20° in [**3**]$^{3+}$ to 32.68° in [**4**]$^{3+}$. It is known that the transfer integral between the $\pi$ subunits, and hence the overlap integral varies as the cosine of the torsion angle [32] thus leading to enhanced push–pull effects towards the withdrawing nitrosyl at lower angle values. The extent of this effect is limited here, and varies from 0.87 (cos 29.20°) to 0.84 (cos 32.68°). Nevertheless, it suggests that having a fluorenylpyridine in *trans*-position with respect to the Ru(NO) fragment ([**3**]$^{3+}$) leads to a more efficient charge transfer than that observed in the *cis*-fluorenylpyridine – Ru(NO) ([**2**]$^{3+}$) linkage.

More relevant electronic features can be obtained from the examination of the computed UV–Vis spectra, presented in Fig. 1. The fluorene-containing complexes [**1**]$^{3+}$, [**2**]$^{3+}$, [**3**]$^{3+}$, and [**4**]$^{3+}$ exhibit three bands located in the 400–450 nm (Band 1), 325–375 nm (Band 2), and 250–300 nm (Band 3) domains. It must be pointed out that Band 1 is present in complex [**2**]$^{3+}$, even though its intensity is very low, but is absent in the fluorene-free complex [**5**]$^{3+}$. This suggests that the fluorene substituent is significantly involved in the low-energy Band 1 and probably in Band 2. It can be seen from Fig. 1 that the high energy Band 3 arises from the contribution of numerous transitions. Their examination reveals that they involve orbitals located on the terpyridine and bipyridine ligands, without any significant contribution of the nitrosyl ligand. Consequently, they are probably not directly involved in the NO release process and therefore will not be described in more details here, for the sake of simplification.

The analysis of Bands 1 and 2 is provided in Table 2. The four ([**1**]$^{3+}$–[**4**]$^{3+}$) complexes based on fluorene exhibit interesting similarities. In particular, the donating character of the fluorene substituent clearly appears in the Table, the electron density being strongly located on the fluorene unit, at the occupied level, in any transition. The resulting charge transfer occurs from the fluorene to the rest of the complex providing a significant push–pull effect in any case. Furthermore, the charge transfer is directed towards the Ru(NO) withdrawing unit only, in Band 1. With this respect, the properties of the four complexes are reminiscent of those of the parent [**1**]$^{3+}$ species, previously reported [15].

It is worth pointing out that the very weak 1 → 3 transition ($f$ = 0.034) of [**2**]$^{3+}$ still exhibits the same fluorene → Ru(NO) charge transfer transition. The reason for its unexpectedly low intensity can be found in Fig. 2, where the orbitals involved in the computed spectra are drawn. The dominant contribution to the main transitions of Band 1 (red arrows in Fig. 2) indicates a net charge transfer from the$\pi$-conjugated fluorene to the $d$(Ru)-$\pi^*$(NO) orbital fragment, in any case. Nevertheless, it is apparent that the $d$ orbital points towards the fluorenyl substituted pyridine in [**1**]$^{3+}$, [**3**]$^{3+}$, and [**4**]$^{3+}$, thus allowing a sizeable Ru-N$_{pyridine}$ overlap and hence an efficient ligand-NO charge transfer, through the metal center. The situation is different in [**2**]$^{3+}$, in which the $d$ orbital is grossly orthogonal with the $\pi$ system of the ligand. Therefore, the overlap is far reduced in this case, the charge transfer hampered with the

**Table 1**
DFT computed parameters for the ruthenium nitrosyl complexes: ruthenium-pyridine (Ru–N) distance in Å, ruthenium-nitrosyl (Ru–NO) distance in Å, torsion angle in degree between the fluorene and the bipyridine planes ($\alpha_{F/B}$) and between the fluorene and the terpyridine plane ($\alpha_{F/T}$).

| Complex | Ru–N$_{terpy}$ | | Ru–N$_{bpy}$ | | Ru–NO | $\alpha_{F/B}$ | $\alpha_{F/T}$ |
|---|---|---|---|---|---|---|---|
| | Central py | Lateral py | *cis* Ru-NO | *trans* Ru-NO | | | |
| [**1**]$^{3+}$ | 1.989 | 2.105<br>2.103 | 2.117 | 2.096 | 1.769 | | 31.54 |
| [**2**]$^{3+}$ | 1.999 | 2.102<br>2.103 | 2.108 | 2.096 | 1.769 | 32.14 | |
| [**3**]$^{3+}$ | 1.998 | 2.103<br>2.107 | 2.115 | 2.081 | 1.772 | 29.20 | |
| [**4**]$^{3+}$ | 1.999 | 2.102<br>2.102 | 2.107 | 2.083 | 1.771 | 32.68 (*cis*)<br>31.28 (*trans*) | |
| [**5**]$^{3+}$ | 1.997 | 2.102<br>2.102 | 2.115 | 2.095 | 1.770 | | |

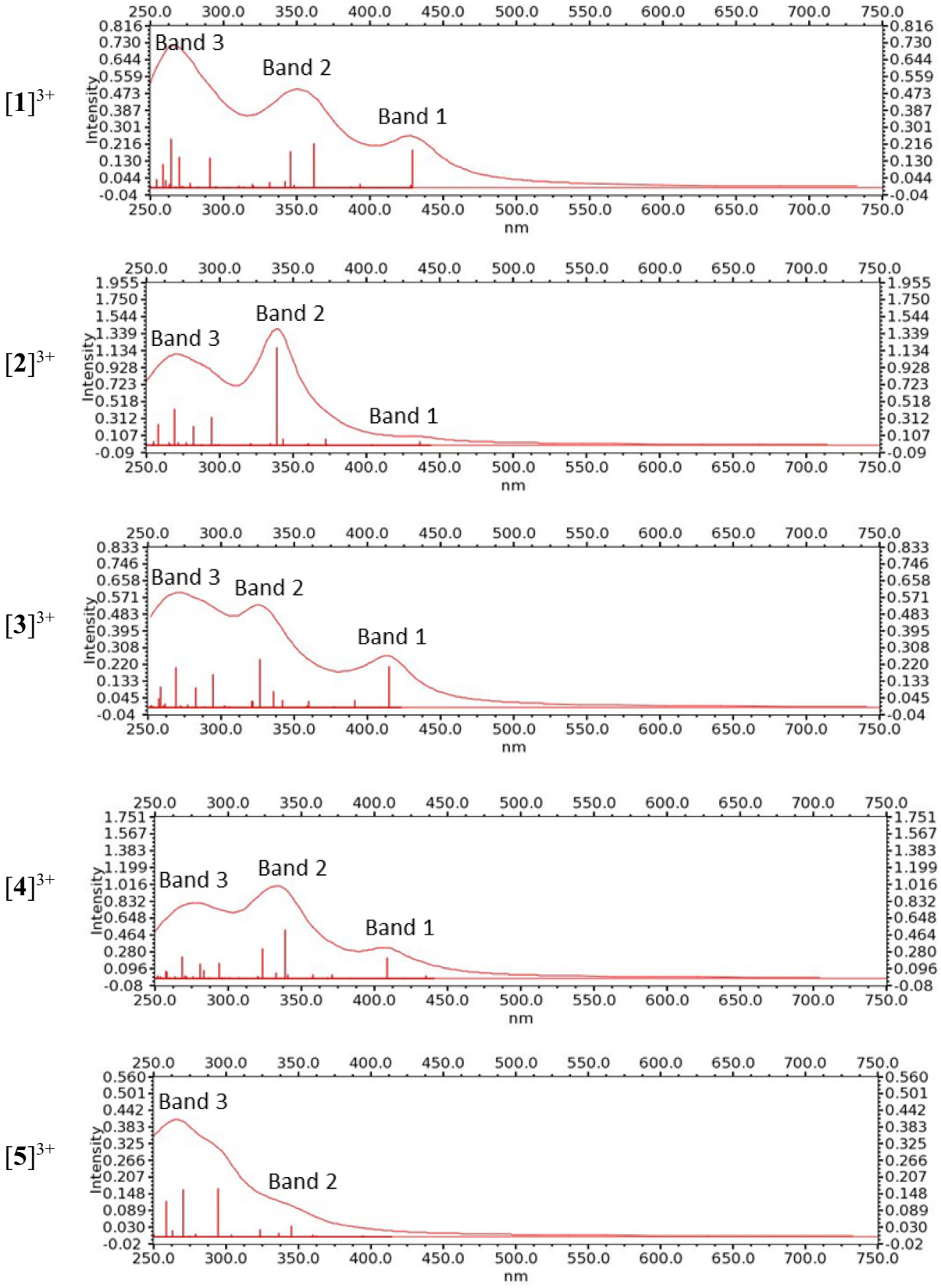


**Fig. 1.** DFT computed UV–Vis spectra at the CAM-B3LYP/6-31G* level for the five ([**1**]$^{3+}$–[**5**]$^{3+}$) complexes, with bands located in the 400–450 nm (Band 1), 325–375 nm (Band 2), and 250–300 nm (Band 3) wavelengths range.

**Table 2**
Main electron transitions, with absorption maxima ($\lambda_{max}$) oscillator strength ($f$) and composition of the configuration interaction, computed by TD-DFT for the five $[\mathbf{1}]^{3+}$–$[\mathbf{5}]^{3+}$ complexes.

| Compounds | Transitions | $\lambda_{max}$ (nm) | $f$ | Main composition[a] | | Character |
|---|---|---|---|---|---|---|
| $[\mathbf{1}]^{3+}$ | Band 1 | 1 → 2 | 430 | 0.314 | 78.4% $\chi_{167\rightarrow168}$ | fluorene → Ru(NO) |
| | Band 2 | 1 → 7 | 362 | 0.370 | 31.2% $\chi_{167\rightarrow170}$ + 18.8% $\chi_{164\rightarrow169}$ + 14.2% $\chi_{159\rightarrow169}$ | fluorene → terpyRu(NO) |
| | | 1 → 9 | 346 | 0.301 | 46.1% $\chi_{167\rightarrow170}$ + 20.9% $\chi_{164\rightarrow169}$ | fluorene → terpyRu(NO) |
| $[\mathbf{2}]^{3+}$ | Band 1 | 1 → 3 | 437 | 0.034 | 58.4% $\chi_{167\rightarrow169}$ + 21.1% $\chi_{160\rightarrow169}$ | fluorene → Ru(NO) |
| | Band 2 | 1 → 10 | 339 | 0.978 | 68.2% $\chi_{167\rightarrow171}$ | fluorene → bpy |
| $[\mathbf{3}]^{3+}$ | Band 1 | 1 → 3 | 415 | 0.350 | 71.3% $\chi_{167\rightarrow169}$ | fluorene → Ru(NO) |
| | Band 2 | 1 → 11 | 327 | 0.417 | 46.9% $\chi_{167\rightarrow171}$ + 10.2% $\chi_{167\rightarrow169}$ + 7.4% $\chi_{163\rightarrow169}$ | fluorene → bpy |
| $[\mathbf{4}]^{3+}$ | Band 1 | 1 → 5 | 409 | 0.367 | 50.0% $\chi_{217\rightarrow220}$ + 32.7% $\chi_{218\rightarrow220}$ | fluorene(*trans*) → Ru(NO) |
| | Band 2 | 1 → 12 | 339 | 0.876 | 58.5% $\chi_{218\rightarrow222}$ + 6.5% $\chi_{218\rightarrow225}$ | fluorene(*cis*) → bpy |
| | | 1 → 14 | 324 | 0.532 | 54.1% $\chi_{217\rightarrow222}$ + 9.2% $\chi_{217\rightarrow220}$ | fluorene(*trans*) → bpy |
| $[\mathbf{5}]^{3+}$ | Band 2 | 1 → 7 | 345 | 0.058 | 59.0% $\chi_{116\rightarrow117}$ + 14.2% $\chi_{112\rightarrow117}$ | terpy → Ru(NO) |

[a] Orbital 167(168) is the HOMO(LUMO) in $[\mathbf{1}]^{3+}$, $[\mathbf{2}]^{3+}$, and $[\mathbf{3}]^{3+}$; Orbital 218(219) is the HOMO(LUMO) in $[\mathbf{4}]^{3+}$; Orbital 116(117) is the HOMO(LUMO) in $[\mathbf{5}]^{3+}$.

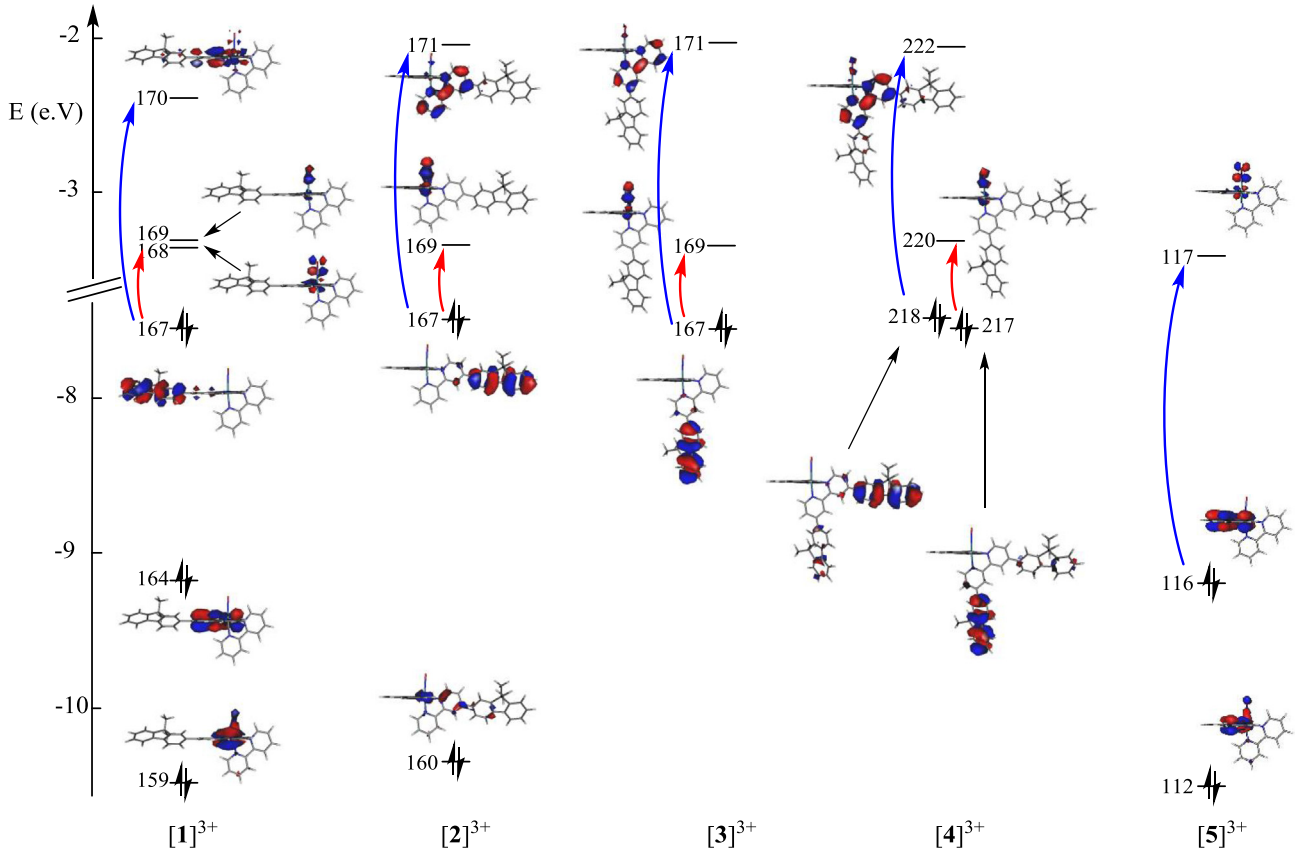


**Fig. 2.** Description and relative energies of the main orbitals involved in the transitions computed for Band 1 (red) and Band 2 (blue) in the [**1**]–[**5**] series. The orbital numbering corresponds to that of Table 2. (Colour online.)

deleterious effect of a dramatic lowering of intensity. Although the full understanding of the mechanism involved in the NO release remains a challenging issue for theorists [33], it may be anticipated that two criteria should determine if a transition is expected to contribute efficiently to the release: (i) a sizeable electron density located on the Ru(NO) fragment in the excited state, leading to a charge transfer effect involving the nitrosyl, and (ii) a strong intensity for the afferent transition. Along this line, $[\mathbf{2}]^{3+}$, does not seem to be a suitable candidate for an efficient NO· release.

The main transitions contributing to Band 2 are compared in Fig. 2 for the ruthenium complexes (blue arrows). While the occupied level is the same in any case (fluorene), the unoccupied level is located on the ligand, either terpyridine ($[\mathbf{1}]^{3+}$) or bipyridine ($[\mathbf{2}]^{3+}$–$[\mathbf{4}]^{3+}$) on which the fluorene is attached. The nitrosyl ligand is weakly involved in these transitions and therefore the contribution of Band 2 in the NO release process seems to be reduced versus that of Band 1.

The situation encountered in $[\mathbf{5}]^{3+}$, where no Band 1 is observed, is significantly different. Due to the absence of fluorene, the extent of the push–pull effect is far reduced in this case, and the charge transfer transitions are blue-shifted. Therefore, the electronic features of Band 2 in $[\mathbf{5}]^{3+}$ which correspond to a terpyridine → Ru(NO) charge transfer (Fig. 2) appear to be a transposition of those of Band 1 in $[\mathbf{1}]^{3+}$–$[\mathbf{4}]^{3+}$ (fluorene → Ru(NO) charge transfer).

From this examination of the computational data available, it can be inferred that the presence of a fluorene in *cis*- position (complex $[\mathbf{2}]^{3+}$) should not provide any improvement of the situation encountered in the reference complex $[\mathbf{1}]^{3+}$, for reason related to the pseudo orthogonality of the $\pi$-fragment orbital of the pyridine and the d orbital of the ruthenium atom. Therefore, the only

fluorenylbipyridine- based complexes of interest are $[\mathbf{3}]^{3+}$ and $[\mathbf{4}]^{3+}$, on which the trans fluorene-pyridine-Ru(NO) linkage is present and reminiscent of that on $[\mathbf{1}]^{3+}$. For the sake of simplification in the synthetic approach, the 4,4′-bisfluorenyl-2,2′-bipyridine based complex $[\mathbf{4}]^{3+}$ has been preferred. Its properties are presented in the next sections and compared to those of $[\mathbf{1}]^{3+}$.

### 3.2. Synthesis and characterization

The introduction of butyl chains on the fluorenyl units of $[\mathbf{4}]^{3+}$ is justified to enhance the solubility in organic solvents and in particular in acetonitrile in relation to the TPA experiments by the Z-scan technics which require concentrated solutions for compounds with moderate values of cross-section. Nevertheless, our previous investigation has shown that the electronic properties (UV–Vis spectra, NO release capabilities, and likely the TPA cross-section) remain essentially unchanged by the presence of these chains, which are not engaged in the long range π-delocalizations responsible for the intramolecular charge transfer effects [15]. Numerous reports have appeared in the literature, devoted to the synthesis of 4,4′-bisfluorenyl-2,2′-bipyridine with alkyl chains of various lengths [34–37], in which the synthetic methodologies are basically the same and differ from the choice of reagents and solvents. In the case of F2B, the procedure employed was that described by Han et al. [19], using 9,9′-dibutyl-9H-fluorene-2-yl boronic acid for the Suzuki coupling, followed by a purification by chromatography on silica (80:20 pentane/ether).

The selected target $[\mathbf{4}](PF_6)_3$ was obtained in three steps starting from $[Ru^{III}(terpy)Cl_3]$ (Scheme 2). While the bipyridine was easily coordinated to the ruthenium for the synthesis of the reference $[\mathbf{5}](PF_6)_3$, as previously reported by Meyer et al. [26], the use of F2B in $[\mathbf{4}](PF_6)_3$ raised unexpected difficulties related to its poor solubility in most commonly used solvents for the complexation. Finally, the coordination was achieved in boiling ethylene glycol for two days. The substitution of Cl by $NO_2$ occurred by following the usual method. Then, the conversion of $NO_2$ to NO was obtained in acidic conditions, following a previously reported method, with slight modifications [15]. The evolution of the overall synthesis can easily be monitored by $^1H$ NMR. Indeed, the proton in 6 position on the bipyridine is located in the vicinity of the *X* ligand (*X* = Cl, $NO_2$, NO), and is therefore very sensitive to the substitution occurring at the different steps of the synthesis. The corresponding chemical shifts are equal to 10.24, 9.92 and 9.29 ppm for $[Ru^{II}(terpy)(F2B)(Cl)](Cl)$, $[Ru^{II}(terpy)(F2B)(NO_2)](PF_6)$, and $[Ru^{II}(terpy)(F2B)(NO)](PF_6)_3$ ($[\mathbf{4}](PF_6)_3$), respectively.

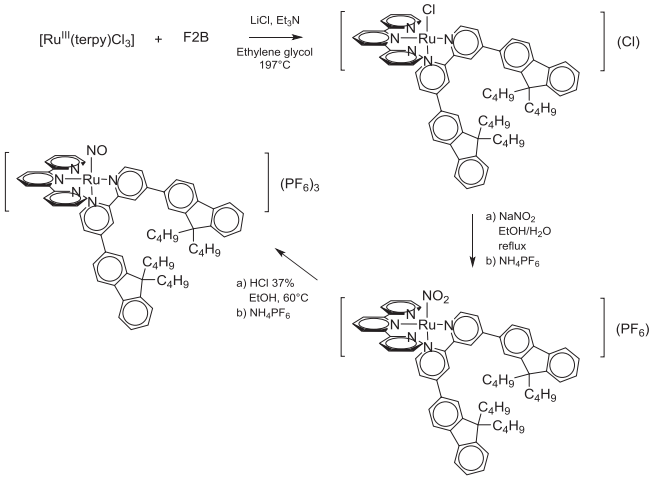


**Scheme 2.** Synthetic route towards $[\mathbf{4}](PF_6)_3$.

Contrary to $[\mathbf{1}](PF_6)_3$ and $[\mathbf{5}](PF_6)_3$, $[\mathbf{4}](PF_6)_3$ was found to be rather unstable in MeCN due to a high sensitivity to trace of water, in neutral pH conditions. Indeed, the complex is subjected to the following reaction:

$$[Ru^{II}(terpy)(F2B)(NO)]^{3+} + 3H_2O \rightleftharpoons [Ru^{II}(terpy)(F2B)(NO_2)]^{+} + 2H_3O^{+} \quad (3)$$

To circumvent this problem, one drop of $HPF_6$ was added to 0.5 mL of deuterated acetonitrile to ensure the quality of the NMR measurement.

The experimental infrared *ν*(NO) stretching frequencies are equal to 1942 $cm^{-1}$, 1943 $cm^{-1}$ and 1958 and 1944 $cm^{-1}$, for $[\mathbf{1}](PF_6)_3$, $[\mathbf{4}](PF_6)_3$, and $[\mathbf{5}](PF_6)_3$, respectively. The *ν*(NO) frequencies arise from internal electronic effects and from solid state effects as well. When internal effects have to be considered, it has been pointed out that the major factor which influences the frequency value is the nature of the ligand in *trans* position with respect to the Ru–NO band [38]. With this respect, $[\mathbf{1}]^{3+}$ and $[\mathbf{5}]^{3+}$ are all built up from the same "pyridine-$Ru^{II}$(NO)" *trans* linkage and therefore are expected to lead to nearly identical *ν*(NO) frequencies values. By contrast, the "fluorenylpyridine-$Ru^{II}$(NO)" *trans* linkage present in $[\mathbf{4}]^{3+}$ exhibits an enhanced push–pull character towards the $\pi^*$ orbitals of the nitrosyl. Consequently, a lower frequency should be expected. The fact that this effect is not observed experimentally indicates that the packing effect is probably dominant in the Ru(NO) series, which can also be anticipated from the observation of two unexpectedly different frequencies in $[\mathbf{5}](PF_6)_3$.

### 3.3. Crystal structure of F2B

F2B crystallizes in the C2/c monoclinic space group. The molecular structure, shown in Fig. 3 arises from two asymmetric unit cells related by an inversion center. Each molecule is weakly linked to 4 neighboring species through 12C···H short contacts in the 2.843(3)–2.856(3) Å range. These interactions involve the 9,9′-dibutyl-9H-fluoren-2-yl substituents only, letting the bipyridine unit free of any interaction. Therefore, the bipyridine ring is almost perfectly planar with a longest distance of 0.016 Å, observed at C(25) to the averaged plane (12 atoms). The fluorene rings are planar with a longest distance of 0.065 Å observed at C(11) to the averaged mean plane (13 atoms). The torsion angle between the fluorene and bipyridine mean planes is equal to 47.78°.

### 3.4. Spectroscopic data

The UV–Vis spectrum of $[\mathbf{4}](PF_6)_3$ is shown in Fig. 4, and compared to those of $[\mathbf{1}](PF_6)_3$ and $[\mathbf{5}](PF_6)_3$. The relative intensities of the absorbance bands varies as follows: $[\mathbf{4}](PF_6)_3 > [\mathbf{1}](PF_6)_3 > [\mathbf{5}](PF_6)_3$, which reflects the size of the π-conjugated ligands. The low energy "push–pull" transitions associated to most of the overall electronic features of the species are detailed in Table 3, and compared with the computed data for $[\mathbf{4}](PF_6)_3$ and $[\mathbf{1}](PF_6)_3$, in order to determine the effect of the position of the donating fluorenyl substituents on the ligands. The agreement between computation and experiment is satisfactory with energy differences around 3000 $cm^{-1}$ being acceptable for molecules subjected to strong charge transfer effects in which heavy atoms are present [39]. Nevertheless, the same tendencies are observed on going from $[\mathbf{1}](PF_6)_3$ to $[\mathbf{4}](PF_6)_3$, namely a significant increase in transitions intensities, and a blue shift.

The observation of a low-energy transition is typically associated with the reduction of the energy gap between the occupied level located on the ligand (on the fluorene in $[\mathbf{1}](PF_6)_3$ and $[\mathbf{4}](PF_6)_3$), and the unoccupied level invariably located on the Ru(NO) fragment. With this respect, the push–pull effect along the

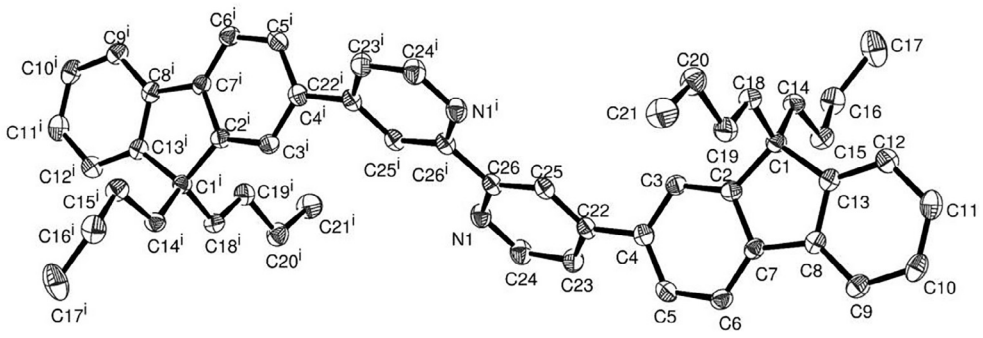


**Fig. 3.** Molecular structure of F2B, showing the two ($N_1$ to $C_{26}$ and $N_{1'}$ to $C_{26'}$) asymmetric units related by an inversion center. Displacement ellipsoids are drawn at the 50% probability level. Hydrogen atoms are omitted for clarity.

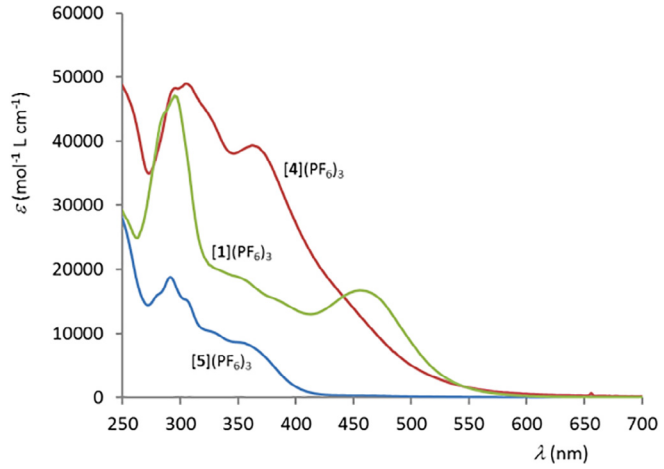


**Fig. 4.** UV–Vis spectra recorded in acetonitrile for Ru(terpy)(bpy) complexes bearing two fluorene ([**4**](PF$_6$)$_3$), one fluorene ([**1**](PF$_6$)$_3$), and no fluorene ([**5**](PF$_6$)$_3$).

**Table 3**
Low energy UV–Vis bands compared to computed transitions for [**4**](PF$_6$)$_3$ and [**1**](PF$_6$)$_3$, with absorption maxima ($\lambda_{max}$ in nm), extinction coefficients ($\varepsilon$ in mol$^{-1}$ L cm$^{-1}$),and oscillator strength ($f$).

| Compound | UV–Vis spectrum | | Computed data | |
|---|---|---|---|---|
| | $\lambda_{max}$ | $\varepsilon$ | $\lambda_{max}$ | $f$ |
| [**4**](PF$_6$)$_3$ | 362 | 39 400 | 409 | 0.367 |
| | 306 | 48 900 | 339 | 0.876 |
| | 296 | 48 300 | 324 | 0.532 |
| [**1**](PF$_6$)$_3$ | 455 | 16 700 | 430 | 0.314 |
| | 350–355 | 18 600 | 362 | 0.370 |
| | 380–390 | 15 100 | 346 | 0.301 |

fluorene-pyridine-Ru(NO) linkage should be the same in both complexes, through the HOMO → LUMO excitation in [**1**](PF$_6$)$_3$, which finds its exact counterpart in the HOMO-1 → LUMO+2 excitation in [**4**](PF$_6$)$_3$. Nevertheless, the data gathered in Table 2 indicate that, while the HOMO → LUMO excitation contributes 78.4% to the whole effect associated to the 1 → 2 low-lying transition in [**1**]$^{3+}$, this contribution is reduced to 50.0% in [**4**]$^{3+}$. Indeed, a second excitation (HOMO → LUMO+2) contributes significantly to the low-lying transition of [**4**](PF$_6$)$_3$. Unfortunately, and as previously discussed for [**2**]$^{3+}$ (Section 3.1.), the orbital fragment of the fluorenylpyridine based HOMO level is roughly orthogonal to the Ru(NO) based LUMO + 2 level in this case, making any charge transfer inoperative and hence reducing the overall push pull effect and red-shift associated to the transition.

### 3.5. NO release capabilities

As previously reported [26], the resulting release of nitric oxide is followed by the formation of a solvent bound ruthenium(III) photoproduct, according to the following equation:

$$(L)Ru^{II} - NO + solvent \xrightarrow{h\nu} (L)Ru^{III} - solvent + NO \quad (4)$$

The suitable wavelength of irradiation is selected for a better consistency with our final target which implies a TPA irradiation at 800 nm (*vide infra*), and hence an absorption observed at 400 nm. Therefore, the one-photon irradiation was performed at 405 nm, which corresponds to a standard experimental setup available in our group. [Note that $\phi_{NO}$, which corresponds to the number of NO• released per [Ru(NO)]* excited states promoted does not depend on the mechanism (either one- or two-photon) employed for the generation of this excited state. Therefore $\phi_{NO}$ is the same at one- and two-photon]. It was determined here at one-photon, for practical reasons.

The changes in the electronic absorption spectrum of [**4**](PF$_6$)$_3$ exposed to 405 nm light in acetonitrile are shown in Fig. 5. The presence of isosbestic points at 264, 368, 442, and 500 nm indicates a clean conversion of the $Ru^{II}(NO^+)$ complexes to related photolysed species. No back-reaction is observed when the light is turned off. In the photolysed species, new bands located at 304, 330, 352 and 468 nm arise. It is interesting to observe that the shape of the final product (red line in Fig. 5) corresponds to a $Ru^{II}$ complex (lack of band at 600 nm characteristic of $Ru^{III}$ species) [26(a)]. This suggests that the photoproduct may be reduced

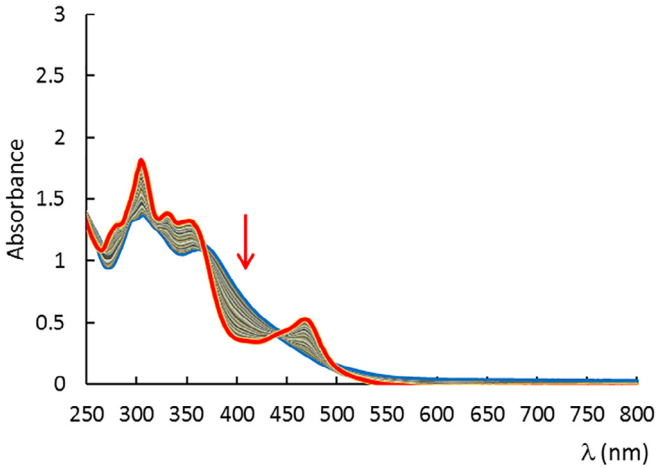


**Fig. 5.** Evolution in the absorption spectra of [**4**](PF$_6$)$_3$ in acetonitrile under irradiation at $\lambda$ = 405 nm (arrow). Blue line: before irradiation; red line: after completeness of the photo-chemical process. (Colour online.)

immediately after the photoreaction, leading to a $Ru^{II}$ complex as the final observable derivative. Nevertheless, the isosbestic points evidenced in Fig. 5 indicate that this second step process is probably extremely fast. Similar features have been reported in other ruthenium-nitrosyl species [40].

The quantum yield of NO release ($\phi_{NO}$) observed for [**4**]$(PF_6)_3$ is equal to 0.033 under light irradiation at 405 nm. This value is on the same order of magnitude of other ruthenium nitrosyl complexes with terpyridine and bipyridine based ligands [40].

Moreover, the photo-generation of NO can be demonstrated experimentally, by EPR spectroscopy under standard excitation, since spin trapping combined with EPR spectroscopy is considered as one of the best methods for the direct detection of NO radicals [41]. Namely, we used Iron(II)-N-methyl-D-glucamine dithiocarbamato $[Fe^{II}(MGD)_2]$ to trap NO due to its high probability of adduct formation and to the high stability of its spin adduct. The appearance of the characteristic triplet signal of NO is shown in Fig. 6, with a hyperfine splitting constant value of $a_N = 1.19 \times 10^{-3}$ $cm^{-1}$ and a g-factor equal to 2.040. These values are fully consistent with the literature report for $[Fe^{II}(MGD)_2\text{-NO}]$ adduct [42]. The weak signal observed in the control spectrum (top of Fig. 6) is due to a trace of NO· and related to the fact that the manipulation is never strictly conducted in the dark.

More convincing experimental features are available from electrochemistry. The voltammograms have been recorded for [**4**]$(PF_6)_3$ and for its related photolyzed product. The results are gathered in Table 4 and displayed in Fig. 7. The $Ru^{II}(NO)$ complex exhibits a reversible reduction wave at +0.43 V (*vs* SCE) ascribed to the $Ru^{II}NO^+ \rightarrow Ru^{II}NO$ reduction according to previous reports on polypyridine $Ru^{II}(NO)$ systems [43–47]. Another two reduction waves at −1.16 V and −1.46 V can be assigned to terpyridine and F2B ligands. Furthermore, the complex is oxidized irreversibly at +1.79 V. This irreversible process is observed in both [**4**]$(PF_6)_3$ and F2B reference species as well, and is therefore attributed to the oxidation of the ligand. The $Ru^{III}/Ru^{II}$ redox couple, usually switched to very high potential in related species due to the strong withdrawing effect of ligand $NO^+$ ligand [43,48,49], cannot be observed and attributed accurately here in the conditions of the experiment, as it falls at the upper limit of the electrochemical window of the solvent. The voltammograms of the photolyzed complex appear deeply modified by irradiation at 405 nm, with three main features summarized as follows: (i) the wave ascribed to the reduction of $NO^+$ into NO· is absent, which indicates complete NO release after irradiation. As the potential falls to +0.20 V, the wave observed at around +0.3 V corresponds to an oxidation process, precluding the possibility of a remaining trace of $NO^+$. Moreover; (ii) the oxidation of the F2B ligand observed at +1.79 V remains grossly unaffected after NO release. This behavior is consistent with the computational analysis of the HOMO level in [**4**]$(PF_6)_3$ (*vide supra*). Indeed, the electron density is fully localized on the fluorenyl fragment at the HOMO level, far away from the Ru(NO) core. Therefore, and to a large extent, we may infer that the release of the NO· radical will have a very modest influence on the HOMO of the ruthenium complex, and hence on its oxidation potential. Finally (iii) a fully reversible oxidation wave observed at +1.25 V, in a range of potential typical of that of an oxidation of $Ru^{II}$ into $Ru^{III}$ species free of $NO^+$ [47,50].

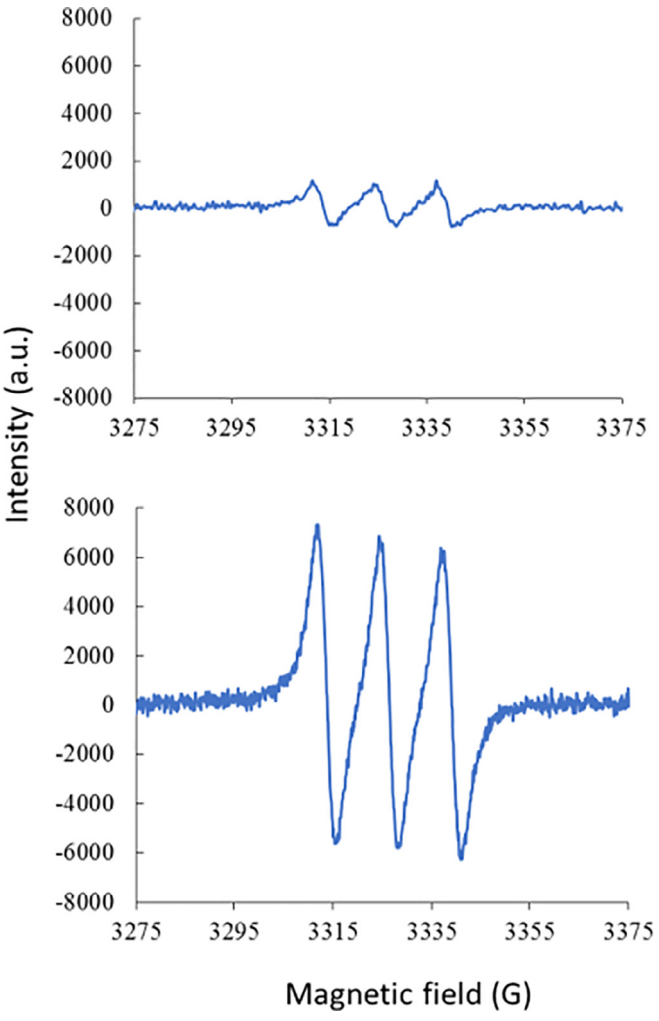


**Fig. 6.** Triplet EPR signals from NO trapped by $[Fe(MGD)_2]$ for [**4**]$(PF_6)_3$ upon one photon excitation at room temperature and at $\lambda > 400$ nm (Hg lamp) (bottom), and control signal before irradiation (top).

### 3.6. TPA properties

Z-scan technique with optical excitation of short pulses (800 nm) was employed to quantify the TPA properties. The use of other spectroscopic techniques to characterize the optical nonlinearities, i.e., two-photon excited fluorescence (TPEF), were precluded as [**4**]$(PF_6)_3$ is not a fluorescent material. Within the present experimental conditions, the simultaneous absorption of two photons at the incident wavelength of 800 nm leads to an equivalent one photon electronic transition of 400 nm, which does not correspond to the absorption maxima of the ruthenium complexes (455 nm and 362 nm, for [**1**]$(PF_6)_3$ and [**4**]$(PF_6)_3$), respectively. Nevertheless, and apart from the fact that two-photon electronic spectra may be significantly different than one-photon spectra, the 800 nm wavelength was selected for practicity as Z-scan experiments with short optical pulses require the use of Ti-sapphire lasers whose emission is precisely around 800 nm. Further, this wavelength is within the window of biomedical interest for medical therapy based on light. Of course, extending the laser emission to other wavelength would be possible but it cannot be envisioned practically, for a question of high cost when laser sources of short pulses are used.

At the molecular level, the quantification of the TPA properties is expressed by a cross-section ($\sigma_{TPA}$), expressed in Göppert-Mayer units (1 GM = $10^{-50}$ $cm^4$ s $photons^{-1}$ $molecules^{-1}$). With Z-scan we measured the nonlinear absorption coefficient ($\beta$) in acetonitrile solutions of [**4**]$(PF_6)_3$ at the concentration of $10^{-2}$ $mol.L^{-1}$. Samples of high concentrations are necessary in Z-scan to assure traces of transmission detected at the far field with good signal to noise ratio. Although [**4**]$(PF_6)_3$ appears transparent at wavelengths longer than 650 nm, in the condition of UV–Vis experiment (Fig. 4), we observed a residual absorption with an absorbance of 0.025 at 800 nm. The presence of residual absorption is not desir-

**Table 4**
Electrochemical data ($E^{1/2}$ *vs* SCE) for [**4**](PF$_6$)$_3$, before and after irradiation at 405 nm. Data for F2B are given as a reference.

| Compounds | Before irradiation | | | | After irradiation | | | |
|---|---|---|---|---|---|---|---|---|
| | $E_{eq}$ | Reduction | | Oxidation | $E_{eq}$ | Reduction | Oxidation | |
| | | $NO^+/NO^·$ | terpy and F2B | F2B | | terpy and F2B | $Ru^{III/II}$ | F2B |
| [**4**](PF$_6$)$_3$ | 0.44 | 0.43 | −1.16<br>−1.46 | 1.79 | 0.20 | −1.28<br>−1.50<br>−1.70<br>−1.93 | 1.25 | 1.79 |
| F2B | | | | 1.77 | | | | |

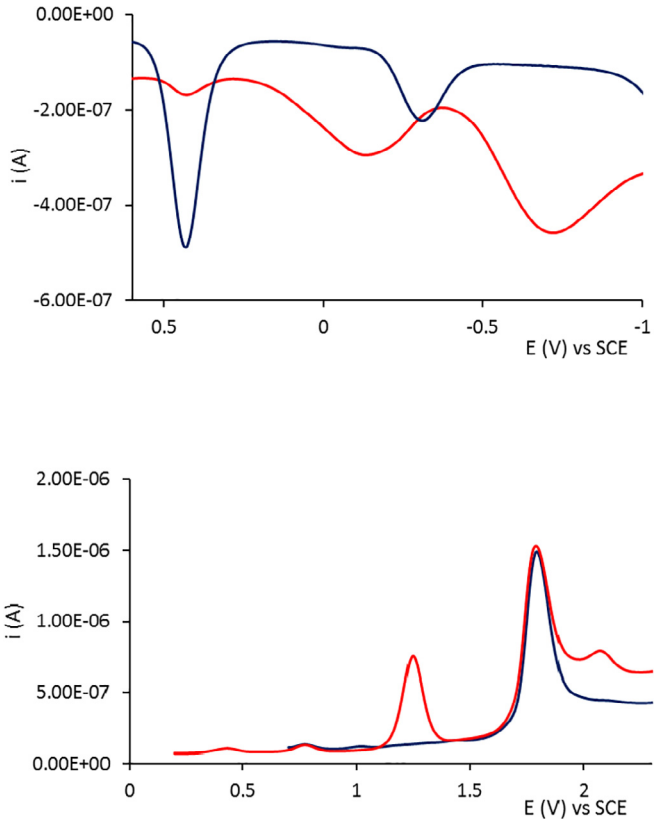


**Fig. 7.** Square wave voltammograms in reduction (top) and in oxidation (bottom) for [**4**](PF$_6$)$_3$ recorded in acetonitrile + 0.1 mol L$^{-1}$ TBAPF$_6$ before (blue) and after (red) irradiation at 405 nm. (Colour online.)

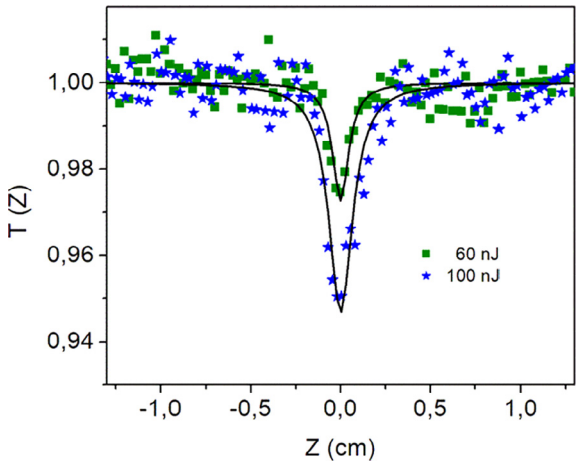


**Fig. 8.** Normalized transmission in Z-scan experiments for [**4**](PF$_6$)$_3$ with different energies of excitation at the wavelength of 800 nm.

able since it can produce thermo-optical effects which in turn distort the Z-scan traces. It should be observed that the residual absorption can also produce some absorption of excited states, but instead of a two-photon transition through a virtual intermediate state, the transition occurs through an intermediate excited state. Therefore, the TPA has two components: intrinsic TPA (via an intermediate virtual state) and two-step excited state absorption. Nevertheless, the use of a very short pulse in the present case (100 fs) with a low repetition rate (1 kHz) is not favorable for the latter type of absorption, then it can be inferred that the Z-scan trace is mostly related to intrinsic TPA in [**4**](PF$_6$)$_3$.

Fig. 8 displays examples of the normalized transmission ($T$(z)) obtained from samples of [**4**](PF$_6$)$_3$ (see Section 2) in Z-scan experiments with optical excitation of 60 and 100 nJ. It is observed that the Z-scan traces exhibit good symmetry around $z = 0$ position (it was verified that the Z-scan traces were not perturbed by undesirable thermo-optical effects for the range of laser intensities used in these experiments). Fig. 8 shows clearly the distinctive nonlinear absorption effect in [**4**](PF$_6$)$_3$: normalized transmission decreased as the intensity of pulses was increased. Experimental data was then fitted using the mathematical formalism for TPA in Z-scan experiments [30]. The nonlinear absorption coefficient ($\beta$) showed a negligible dependence on the energy of excitation for the range of energies employed in the Z-scan experiments. The average $\beta$ for [**4**](PF$_6$)$_3$ and the corresponding $\sigma_{TPA}$ from a total of 15 plots resulted in the values shown in Table 5. This Table also shows the $\beta$ and $\sigma_{TPA}$ values for the fluorene-based parent compound [**1**](PF$_6$)$_3$.

As a concluding remark, it is important to point out that the parameter of interest in TPA induced drug delivery is neither the cross-section ($\sigma_{TPA}$), nor the quantum yield of photo release ($\phi_{NO}$), but rather the $\sigma_{TPA} \times \phi_{NO}$ product regarded as an "uncaging parameter", which links the number of NO· generated to the number of photon delivered to the sample. The resulting uncaging parameters at 400 nm (one-photon) and 800 nm (two-photon) are shown in Table 6. First, and due to an extended $\pi$-conjugated structure, the absorption are more intense at both one- and two-photon in the case of [**4**](PF$_6$)$_3$. While one- and two-photon absorptions may scale differently, in particular in centrosymmetric chromophores, they are likely to be similar when the push–pull character becomes more pronounced, like in the present case. Finally, it turns out from the examination of Table 5 that both [**1**]

**Table 5**
Nonlinear absorption coefficients ($\beta$), and TPA cross-sections ($\sigma_{TPA}$), for [**1**](PF$_6$)$_3$ and [**4**](PF$_6$)$_3$ at incident laser wavelength of 800 nm.

| Compound | $\beta$ ($10^{-11}$ cm/W) | $\sigma_{TPA}$ (GM) | Refs. |
|---|---|---|---|
| [**1**](PF$_6$)$_3$ | 2.63 ± 0.43 | 108 ± 18 | [15] |
| [**4**](PF$_6$)$_3$ | 3.80 ± 0.59 | 156 ± 23 | This work |

**Table 6**
Uncaging parameters ($\varepsilon \times \phi_{NO}$ at one photon and $\sigma_{TPA} \times \phi_{NO}$ at two-photon) for the NO release observed in [**1**](PF$_6$)$_3$, [**4**](PF$_6$)$_3$.

| Compound | One-photon absorption | | | Two-photon absorption | | |
|---|---|---|---|---|---|---|
| | $\varepsilon$ (400 nm) | $\phi_{NO}$ | $\varepsilon \times \phi_{NO}$ | $\sigma_{TPA}$ (800 nm) | $\phi_{NO}$ | $\sigma_{TPA} \times \phi_{NO}$ |
| [**1**](PF$_6$)$_3$ | 13 700 | 0.06 | 822 | 108 ± 18[a] | 0.06 | 6.48 |
| [**4**](PF$_6$)$_3$ | 27 200 | 0.033 | 898 | 156 ± 23 | 0.033 | 5.14 |

[a] Ref. [15].

(PF$_6$)$_3$ and [**4**](PF$_6$)$_3$ materials exhibit roughly the same uncaging capabilities.

## 4. Conclusion

The strategies developed for enhancing the TPA cross-section and related NO• release capabilities of [**5**](PF$_6$)$_3$ by addition of donating fluorenyl substituents either on the terpyridine ([**1**](PF$_6$)$_3$) or on the bipyridine ([**1**](PF$_6$)$_3$) have been compared theoretically and experimentally. It is demonstrated that the presence of two fluorenes on the bipyridine is not useful, as one of them does not contribute to significant charge transfer effects towards Ru(NO), due to orbitals orthogonality. The extension of the delocalization in the bis-fluorenyl [**4**]$^{3+}$ complex leads to a significant increase (from 108 GM to 156 GM) of the cross-section versus that measured on [**1**]$^{3+}$. On the other hand, the NO• release process is twice less efficient in [**4**]$^{3+}$ than in [**1**]$^{3+}$. This unexpected result presses the need for a clear understanding of the mechanism involved in the NO•, which remains a challenge for theoreticians.

## Acknowledgements

The work has been performed within the framework of the French Mexican International Laboratory LIA-LCMMC. The authors thank CNRS (France) and CONACYT (Mexico) for financial support, Lionel Rechignat (LCC-CNRS) for recording EPR spectra, and Alix Sournia-Saquet (LCC-CNRS) for the electrochemical studies. M.R. thanks MESR (Ministère de l'Enseignement Supérieur et de la Recherche) for a PhD fellowship. V.B. thanks the French Embassy in Kiev and Campus France (Europe, 835930K) for financial support. A.E.C thanks CONACyT for a PhD fellowship (270200).

## Appendix A. Supplementary data

CCDC #1834279 contains the supplementary crystallographic data for F2B. These data can be obtained free of charge via http://www.ccdc.cam.ac.uk/conts/retrieving.html, or from the Cambridge Crystallographic Data Centre, 12 Union Road, Cambridge CB2 1EZ, UK; fax: (+44) 1223-336-033; or e-mail: deposit@ccdc.cam.ac.uk. Supplementary data associated with this article can be found, in the online version, at https://doi.org/10.1016/j.poly.2018.05.028.

## References

[1] (a) L.J. Ignarro, Nitric Oxide Biology and Pathobiology, Academic Press, San Diego, 2000;
(b) B. Bonavida (Ed.), Nitric Oxide and Cancer: Prognosis, Prevention and Therapy, Springer, New-York, 2010;
(c) A.R. Butler, R. Nicholson, Life Death and Nitric Oxide, The Royal Society of Chemistry, Cambridge, 2003.
[2] (a) P.C. Ford, Nitric Oxide 34 (2013) 56;
(b) A.W. Carpenter, M.H. Schoenfisch, Chem. Soc. Rev. 41 (2012) 3742.
[3] E. Tfouni, D.R. Truzzi, A. Tavares, A.J. Gomes, L.E. Figueiredo, D.W. Franco, Nitric Oxide 26 (2012) 38.
[4] S. Singh, A.K. Gupta, Cancer Chemother. Pharmacol. 67 (2011) 1211.
[5] A.J. Burke, F.J. Sullivan, F.J. Giles, S.A. Glynn, Carcigenesis 34 (2013) 503.
[6] S. Mocellin, V. Bronte, D. Nitti, Med. Res. Rev. 27 (2007) 317.
[7] J.C. Toledo, O. Augusto, Chem. Res. Toxicol. 25 (2012) 975.
[8] For a recent entry to the world of metal nitrosyl complexes, see: Structure and Bonding (Berlin, Germany) special issue on "Nitrosyl Complexes in Inorganic Chemistry, Biochemistry and Medicine", vol. 153 and 154 (2014).
[9] (a) S.Y. Shaban, R. van Eldik, J. Coord. Chem. 70 (2017) 1713;
(b) R. Pulukkody, R.B. Chupik, S.K. Montalvo, S. Khan, N. Bhuvanesh, S.M. Lim, M.Y. Darensbourg, Chem. Commun. 53 (2017) 1180;
(c) F. Wittkamp, C. Nagel, P. Lauterjung, B. Mallick, U. Schatzschneider, U.P. Apfel, Dalton Trans. 45 (2016) 10271;
(d) J. Bhuyan, S. Sarkar, Sabyasachi, Chem. Asian J. 7 (2012) 2690;
(e) Y.J. Chen, W.C. Ku, L.T. Feng, M.L. Tsai, C.H. Hsieh, W.H. Hsu, W.F. Liaw, C.H. Hung, Y.J. Chen, J. Am. Chem. Soc. 130 (2008) 10929;
(f) A.A. Eroy-Reveles, C.G. Hoffman-Luca, P.K. Mascharak, Dalton Trans. 45 (2007) 5268;
(g) A.K. Patra, R.K. Afshar, M.M. Olmstead, P.K. Mascharak, Angew. Chem., Int. Ed. 41 (2002) 2512;
(h) P.C. Ford, J. Bourassa, K. Miranda, B. Lee, I. Lorkovic, S. Boggs, S. Kudo, L. Laverman, Coord. Chem. Rev. 171 (1998) 185.
[10] (a) Y. Hitomi, Y. Iwamoto, M. Kodera, Dalton Trans. 43 (2014) 2161;
(b) W. Zheng, S. Wu, S. Zhao, Y. Geng, J. Jin, Z. Su, Q. Fu, Inorg. Chem. 51 (2012) 3972;
(c) B.J. Heilman, G.M. Halpenny, P.K. Mascharak, Pradip, J. Biomed. Mater. Res., Part B: Appl. Biomat. 99 (2011) 328;
(d) C.G. Hoffman-Luca, A.A. Eroy-Reveles, J. Alvarenga, P.K. Mascharak, Inorg. Chem. 48 (2009) 9104;
(e) A.A. Eroy-Reveles, Y. Leung, C.M. Beavers, M.M. Olmstead, P.K. Mascharak, J. Am. Chem. Soc. 130 (2008) 4447;
(f) A.A. Eroy-Reveles, Y. Leung, P.K. Mascharak, J. Am. Chem. Soc. 128 (2006) 7166;
(g) K. Ghosh, A.A. Eroy-Reveles, T.R. Holman, M.M. Olmstead, P.K. Mascharak, Inorg. Chem. 43 (2004) 2988;
(h) K.J. Franz, S.J. Lippard, Inorg. Chem. 39 (2000) 3722.
[11] (a) N.L. Fry, P.K. Mascharak, Acc. Chem. Res. 44 (2011) 289;
(b) M.J. Rose, P.K. Mascharak, Coord. Chem. Rev. 252 (2008) 2093;
(c) M.J. Rose, P.K. Mascharak, Curr. Opin. Chem. Biol. 12 (2008) 238.
[12] (a) E. Tfouni, M. Krieger, B.R. McGarvey, D.W. Franco, Chem. Coord. Rev. 236 (2003) 57;
(b) E. Tfouni, D.R. Truzzi, A. Tavares, A.J. Gomes, L.E. Figueiredo, D.W. Franco, Nitric Oxide 26 (2012) 38.
[13] (a) For recent reports on NO release from ruthenium nitrosyl complexes, see: M. Guo, H.J. Xiang, Y. Wang, Q.L. Zhang, L. An, S.P. Yang, Y. Ma, Y. Wang, J.G. Liu Chem. Commun. 53 (2017) 3253;
(b) G.L.S. Rodrigues, W.R. Rocha, J. Phys. Chem. B 120 (2016) 11821;
(c) H.J. Xiang, M. Guo, L. An, S.P. Yang, Q.L. Zhang, J.G. Liu, J. Mater. Chem. B 4 (2016) 4667;
(d) N. Cacita, B. Possato, C.F.N. da Silva, C.M. Paulo, A.L.B. Formiga, L.M. Bendhack, S. Nikolaou, Inorg. Chim. Acta 429 (2015) 114;
(e) J.C.M. Pereira, M.L. Souza, D.W. Franco, Eur. J. Inorg. Chem. 2015 (2015) 1005;
(f) K. Ghosh, R. Kumar, K. Kumar, A. Ratnam, U.P. Singh, RSC Adv. 4 (2014) 43599.
[14] M.R. Hamblin, T. N. Demidova, Proc. SPIE, Mechanism for Low-Light Therapy 6140 (2006) 614001.
[15] A. Enriquez-Cabrera, I. Sasaki, V. Bukhanko, M. Tassé, S. Mallet-Ladeira, P.G. Lacroix, R.M. Barba-Barba, G. Ramos, N. Farfán, Z. Voitenko, I. Malfant, Eur. J. Inorg. Chem. (2017) 1446.
[16] (a) Among many recent uses of fluorene in TPA materials, see: J.B. Verlhac, G. Clermont, M. Blanchard-Desce J. Porph. Phthal. 21 (2017) 77;
(b) Ch. Tran, N. Berqouch, H. Dhimane, G. Clermont, M. Blanchard-Desce, D. Ogden, P.I. Dalko, Chem. Eur. J. 23 (2017) 1860;
(c) R. Liu, M. Shu, J. Hu, S. Zhu, H. Shi, H. Zhu, Dyes Pigments 137 (2017) 174;
(d) S.A. Kurhuzenkau, A.W. Woodward, S. Yao, K.D. Belfield, Y.O. Shaydyuk, C. Sissa, M.V. Bondar, A. Painelli, Phys. Chem. Chem. Phys. 18 (2016) 12839;
(e) V. Kundi, P.P. Thankachan, J. Phys. Chem. A 120 (2016) 2757;
(f) L. Yan, X. Linyin, L. Yan, H. Andong, R. Sheng, Huang, Phys. Chem. Chem. Phys. 18 (2016) 4134;
(g) X. Shen, S. Li, L. Li, S.Q. Yao, Q.H. Xu, Chem. Eur. J. 21 (2015) 2214.
[17] (a) For reviews on TPA molecular materials and applications, see: B. Strehmel, V. Strehmel Adv. Photochem. 29 (2007) 111;
(b) G.S. He, L.S. Tan, Q. Zheng, P.N. Prasad, Chem. Rev. 108 (2008) 1245;
(c) M. Pawlicki, H.A. Collins, R.G. Denning, H.L. Anderson, Angew. Chem., Int. Ed. 48 (2009) 3244.
[18] (a) For selected examples of TPA molecules with applications in photodynamic therapy, see: M.A. Oar, W.R. Dichtel, J.M. Serin, J.M.J. Fréchet,

J.E. Rogers, J.E. Slagle, P.A. Fleitz, L.S. Tan, T.Y. Ohulchanskyy, M.N. Prasad Chem. Mater. 18 (2006) 3682;
(b) S. Kim, T.Y. Ohulchanskyy, H.E. Pudavar, R.K. Pandey, P.N. Prasad, J. Am. Chem. Soc. 129 (2007) 2669;
(c) M. Khurana, H.A. Collins, A. Karotki, H.L. Anderson, D.T. Cramb, B.C. Wilson, Photochem. Photobiol. 83 (2007) 1441;
(d) K.S. Samkoe, A.A. Clancy, A. Karotki, B.C. Wilson, D.T. Cramb, J. Biol. Opt. 12 (2007), 034025/034021-034025/034014;
(e) J.R. Starkey, A.K. Rebane, M.A. Drobizev, F. Meng, A. Gong, A. Elliot, K. McInnerney, C.W. Spangler, Clin. Cancer Res. 14 (2008) 6564;
(f) L. Beverina, M. Crippa, M. Landenna, R. Ruffo, P. Salice, F. Silvestri, S. Versari, A. Villa, L. Ciaffoni, E. Collini, C. Ferrante, S. Bradamante, C.M. Mari, R. Bozio, G. A. Pagani, J. Am. Chem. Soc. 130 (2008) 1894;
(g) H.A. Collins, M. Khurana, E.H. Moriyama, A. Mariampillai, E. Dahlstedt, M. Balaz, M.K. Kuimova, M. Drobizhev, V.X.D. Yang, D. Phillips, A. Rebane, B.C. Wilson, H.L. Anderson, Nat. Photonics 2 (2008) 420.
[19] W.S. Han, J.K. Han, H.Y. Kim, M.J. Choi, Y.S. Kang, C. Pac, S.O. Kang, Inorg. Chem. 50 (2011) 3271.
[20] (a) K.J. Takeuchi, M.S. Thompson, D.W. Pipes, T.J. Meyer, Inorg. Chem. 23 (1984) 1845;
(b) W.R. Murphy Jr., K. Takeuchi, M.H. Barley, T.J. Meyer, Inorg. Chem. 25 (1986) 1041.
[21] P.A. Adcock, F. Richard Keene, R.S. Smythe, M.R. Snow, Inorg. Chem. 23 (1984) 2336.
[22] G.M. Sheldrick, Acta Cryst. A71 (2015) 3–8.
[23] G.M. Sheldrick, Acta Cryst. A64 (2008) 112–122.
[24] M.J. Frisch, G.W. Trucks, H.B. Schlegel, G.E. Scuseria, M.A. Robb, J.R. Cheeseman, G. Scalmani, V. Barone, B. Mennucci, G.A. Petersson, H. Nakatsuji, M. Caricato, X. Li, H.P. Hratchian, A.F. Izmaylov, J. Bloino, G. Zheng, J.L. Sonnenberg, M. Hada, M. Ehara, K. Toyota, R. Fukuda, J. Hasegawa, M. Ishida, T. Nakajima, Y. Honda, O. Kitao, H. Nakai, T. Vreven, J.A. Montgomery Jr., J.E. Peralta, F. Ogliaro, M. Bearpark, J.J. Heyd, E. Brothers, K.N. Kudin, V.N. Staroverov, R. Kobayashi, J. Normand, K. Raghavachari, A. Rendell, J.C. Burant, S.S. Iyengar, J. Tomasi, M. Cossi, N. Rega, J.M. Millam, M. Klene, J.E. Knox, J.B. Cross, V. Bakken, C. Adamo, J. Jaramillo, R. Gomperts, R.E. Stratmann, O. Yazyev, A.J. Austin, R. Cammi, C. Pomelli, J.W. Ochterski, R.L. Martin, K. Morokuma, V.G. Zakrzewski, G.A. Voth, P. Salvador, J.J. Dannenberg, S. Dapprich, A.D. Daniels, Ö. Farkas, J.B. Foresman, J.V. Ortiz, J. Cioslowski, D.J. Fox, Gaussian 09, Revision E.01, Gaussian, Inc., Wallingford CT, 2009.
[25] A.W. Ehlers, M. Böhme, S. Dapprich, A. Gobbi, A. Höllwarth, V. Jonas, K.L. Köhler, R. Stegmann, A. Vedkamp, G. Frenking, Chem. Phys. Lett. 208 (1993) 111.
[26] (a) J. Akl, I. Sasaki, P.G. Lacroix, I. Malfant, S. Mallet-Ladeira, P. Vicendo, N. Farfán, R. Santillan, Dalton Trans. 45 (2014) 12721;
(b) J. Akl, I. Sasaki, P.G. Lacroix, V. Hugues, M. Bocé, S. Mallet-Ladeira, P. Vicendo, M. Blanchard Desce, I. Malfant, Photochem. Photobiol. Sci. 15 (2016) 1484.
[27] A.R. Allouche, J. Comput. Chem. 32 (2011) 174.
[28] Program Sa3.3 written by D. Lavabre and V. Pimienta (http://cinet.chim.pagesperso-orange.fr/tele_sa/install_Sa.html).
[29] V. Pimienta, C. Frouté, M.-H. Deniel, D. Lavabre, R. Guglielmetti, J.C. Micheau, J. Photochem. Photobiol. A 122 (1999) 199 (reference 35).
[30] E.W. Van Stryland, M. Sheik-Bahae, in: Characterization Techniques and Tabulations for Organic Nonlinear Materials, Marcel Dekker, Inc., 1998, pp. 655–682.
[31] N.S. Makarov, M. Drobizhev, A. Rebane, Opt. Express 16 (2008) 4029.
[32] R. Chauvin, Ch. Lepetit, Phys. Chem. Chem. Phys. 15 (2013) 3855, and references herein.
[33] J.S. Garcia, F. Alary, Fabienne, M. Boggio-Pasqua, I. Dixon, Isabelle, J.L. Heully, J. Mol. Model. 22 (2016) 1.
[34] (a) G. Koyyada, Ch.P. Pavan, P. Salvatori, G. Marotta, M.G. Lobello, O. Bizzarri, F. de Angelis, C. Malapaka, Inorg. Chim. Acta 442 (2016) 158;
(b) G. Marotta, Ch.P. Kumar, M.G. Lobello, F. Cavazzini, P. Salvatori, K. Ganesh, M.K. Nazeeruddin, M. Chandrasekharam, F. de Angelis, Dalton Trans. 44 (2015) 5369;
(c) M. Chandrasekharam, G. Rajkumar, C.S. Rao, T. Suresh, P.Y. Reddy, J.H. Yum, M.K. Nazeeruddin, M. Graetzel, Adv. Nat. Sci. Nanosci. Nanotechnol. 2 (2011) 035016;
(d) M. Chandrasekharam, G. Rajkumar, T. Suresh, C.S. Rao, P.Y. Reddy, J.H. Yum, M.K. Nazeeruddin, M. Graetzel, Adv Optoelectron. 2011 (2011) 22.
[35] S. Aghazada, P. Gao, A. Yella, G. Marotta, T. Moehl, J. Teuscher, J.E. Moser, F. de Angelis, M. Grätzel, M.K. Nazeeruddin, Inorg. Chem. 55 (2016) 6653.
[36] Y.S. Yen, Y.C. Chen, Y.C. Hsu, H.H. Chou, J.T. Lin, D.J. Yin, Chem. Eur J. 17 (2011) 6781.
[37] Y. Shi, M. Liang, L. Wang, H. Han, L. You, Z. Sun, S. Xue, ACS Appl. Mater. Interfaces. 5 (2013) 144.
[38] (a) See for example: S. Pell, J.N. Armor Inorg. Chem. 12 (1973) 873;
(b) E.E. Mercer, W.A. McAllister, J.R. Durig, Inorg. Chem. 5 (1966) 1881.
[39] A.D. Laurent, D. Jacquemin, Int. J. Quant. Mech. 113 (2013) 2019.
[40] A. Enriquez-Cabrera, P.G. Lacroix, I. Sasaki, S. Malet-Ladeira, N. Farfán, R.M. Barba-Barba, G. Ramos-Ortiz, I. Malfant, Eur. J. Inorg. Chem. (2017) 531.
[41] A.F. Vanin, A.P. Poltorakov, V.D. Mikoyan, L.N. Kubrina, E. van Faassen, Nitric Oxide 15 (2006) 295.
[42] A.J. Liu, Q. Duan, J. Wang, Z. Song, X. Qiao, H. Wang, J. Biomed. Opt. 20 (2015), 015004-1–015004-7.
[43] P. De, B. Sarkar, S. Maji, A.K. Das, E. Bulak, S.M. Mobin, W. Kaim, G.K. Lahiri, Eur. J. Inorg. Chem. 18 (2009) 2702.
[44] A.N. de Carvalho, E.C. Fornari, W.R. Gomes, D.M.S. Araújo, A.E.H. Machado, S. Nikolaou, Inorg. Chim. Acta 370 (2011) 444.
[45] D.W. Pipes, T.J. Meyer, Inorg. Chem. 23 (1984) 2466.
[46] S. Maji, B. Sarkar, M. Patra, A.K. Das, S.M. Mobin, W. Kaim, G.K. Lahiri, Inorg. Chem. 47 (2008) 3218.
[47] S. Sarkar, B. Sarkar, N. Chanda, S. Kar, S.M. Mobin, J. Fiedler, W. Kaim, G.K. Lahiri, Inorg. Chem. 44 (2005) 6092.
[48] R.W. Callahan, T.J. Meyer, Inorg. Chem. 16 (1977) 574.
[49] P. De, T.K. Mondal, S.M. Mobin, B. Sarkar, G. Kumar Lahiri, Inorg. Chim. Acta 363 (2010) 2945.
[50] M.J. Rose, A.K. Patra, E.A. Alcid, M.M. Olmstead, P.K. Mascharak, Inorg. Chem. 46 (2007) 2328.